Society of Medical Education & Research

2025, Volume 5, Issue 1, Page No: 53-74

ISSN: 3108-4834

Archive of International Journal of Cancer and Allied Science

CircRNA EZH2 Forms a FUS/KLF5/CXCR4 Feedback Loop to Promote Epithelial-Mesenchymal Transition and Liver Metastasis in Breast Cancer

Sofia Elena Petrescu[1], Andreea Maria Ionescu[1], Filip Kristian Berg[2], Jonas Erik Nordstrom[2], Elena Gabriela Dumitru[1]

[1]Department of Oncology, University of Bucharest, Bucharest, Romania.
[2]Department of Clinical Cancer Research, University of Oslo, Oslo, Norway.

***E-mail** ✉ s.petrescu.unibuc@yahoo.com

Abstract

Breast cancer metastasis accounts for the majority of cancer-related deaths globally. Recent studies indicate that circRNAs are implicated in both tumor formation and metastatic processes in breast cancer. Yet, the specific mechanisms by which circRNAs regulate liver metastasis of breast cancer remain largely unclear. Microarray profiling of three pairs of primary breast cancer (BC) tissues and corresponding liver metastases identified circEZH2. The presence, characteristics, and expression of circEZH2 were confirmed using RT-qPCR and FISH assays. Functional assays in vitro and in vivo demonstrated that circEZH2 functions as an oncogene promoting metastasis. A combination of bioinformatics, Western blot, RNA pull-down, RIP, ChIP, and animal experiments was applied to delineate a feedback loop comprising FUS, circEZH2, miR-217-5p, KLF5, CXCR4, and epithelial-mesenchymal transition (EMT).Our findings showed that circEZH2 is upregulated in liver metastases of BC and correlates with poorer patient prognosis. Overexpression of circEZH2 significantly enhanced BC cell proliferation and invasion, whereas its knockdown produced the opposite effect. In vivo, circEZH2 overexpression facilitated tumor growth and liver metastasis. Mechanistically, circEZH2 acted as a sponge for miR-217-5p, leading to increased KLF5 expression, which in turn activated FUS transcription and promoted circEZH2 back-splicing. Additionally, KLF5 transcriptionally upregulated CXCR4, accelerating EMT in BC cells. A novel FUS/circEZH2/KLF5/CXCR4 feedback loop was uncovered, suggesting that circEZH2 could serve as a promising biomarker and therapeutic target in BC.

Keywords: CircRNAs, Breast cancer, Metastasis, Feedback loop, EMT

Introduction

Breast cancer (BC) is the most common malignancy among women and remains a leading cause of cancer-related mortality in females worldwide. Recent studies report a 5-year survival rate of nearly 90% for primary BC. However, 33% of BC patients develop distant non-nodal metastases, reducing the 5-year survival rate to 23% [1]. Clinically, BC primarily metastasizes to the lung, bone, and liver, with the liver being the third most frequent metastatic site. Approximately 50% of patients with distant metastases exhibit liver involvement, while 5–12% of patients present liver metastases as the initial recurrent site [2]. Untreated BC liver metastases (BCLM) have a median survival of 4–8 months [3]. Standard treatments, including chemotherapy and/or systemic hormonal therapy, can extend survival to 18–24 months [4-6]. Metastatic tumor cells acquire organ-specific traits to adapt to the liver microenvironment. Studies have shown that low E-cadherin, high Claudin-2, and elevated fibronectin facilitate liver metastasis [7, 8]. Despite this, the role of circRNAs in enhancing BC cell invasiveness during metastasis remains poorly understood.

Only about 2% of the cellular transcriptome encodes mRNAs, while the majority comprises noncoding RNAs

Access this article online https://smerpub.com/

Received: 14 January 2025; **Accepted:** 18 April 2025

How to cite this article: Petrescu SE, Ionescu AM, Berg FK, Nordstrom JE, Dumitru EG. CircRNA EZH2 Forms a FUS/KLF5/CXCR4 Feedback Loop to Promote Epithelial-Mesenchymal Transition and Liver Metastasis in Breast Cancer. Arch Int J Cancer Allied Sci. 2025;5(1):53-74. https://doi.org/10.51847/hjb9pwSOWl

[9]. CircRNAs are abundant in both the cytoplasm and nucleus and participate in diverse regulatory processes. Unlike linear mRNAs, circRNAs lack a 3′-poly-A tail, making them more stable and evolutionarily conserved [10, 11]. CircRNAs are increasingly studied due to their ability to sponge microRNAs (miRNAs), interact with proteins, or even encode novel peptides [12-14]. Dysregulation of circRNAs has been reported in multiple human cancers [15-18], highlighting their potential as biomarkers and therapeutic targets. However, their functional role in promoting BCLM has not been fully defined.

In this study, we identified a novel circRNA, hsa_circ_0008324 (circEZH2), which was markedly upregulated in BCLM and predicted poor survival in BC patients. CircEZH2 promoted tumorigenesis and metastasis in vitro and in vivo by sponging miR-217-5p to upregulate KLF5, while KLF5-mediated transcriptional activation of FUS enhanced circEZH2 back-splicing. Ultimately, KLF5 upregulated CXCR4 to drive EMT in BC cells.

Results and Discussion

CircEZH2 is associated with liver metastasis in BC

To explore circRNAs differentially expressed in BC liver metastases (BCLM), circRNA microarrays were performed on three pairs of primary BC tumors and matched hepatic metastatic tissues. Using the following criteria—(1) P value < 0.005, (2) fold-change ≥ 2, (3) recorded in circBase, deepBase, and the Rybak-Wolf 2015 dataset, (4) gene symbol linked to metastasis according to recent studies, and (5) upregulated in clinical BCLM samples relative to primary BC tissues—circEZH2 (hsa_circ_0008324) was identified among the upregulated circRNAs (**Figures 1a and 1b**). CircEZH2 is composed of three exons (exon 2, exon 3, and exon 4) of EZH2, which are highly conserved across species, including rhesus, mouse, and dog. Sanger sequencing confirmed the back-spliced junction of circEZH2, validating its circular form (**Figure 1c**).

To verify back-splicing, divergent and convergent primers were designed to amplify circEZH2 and linear EZH2, respectively. CircEZH2 was amplified only in cDNA using divergent primers, whereas linear EZH2 was amplified in both gDNA and cDNA with convergent primers, confirming that circEZH2 is indeed a back-spliced circRNA (**Figure 1d**). RNase R assays further demonstrated that circEZH2 resisted exonuclease digestion better than linear EZH2 and GAPDH, supporting its circular structure (**Figure 1e**). Actinomycin D treatment revealed that circEZH2 has a longer half-life than linear EZH2, indicating enhanced stability (**Figure 1h**). These data collectively confirmed that circEZH2 exhibits the characteristics of a stable back-spliced circRNA and could serve as a potential biomarker.

Subcellular fractionation revealed that circEZH2 was predominantly localized in the cytoplasm of BC cells as detected by RT-qPCR (**Figure 1f**). This cytoplasmic distribution was further confirmed using FISH with a Cy3-labeled circEZH2 probe (**Figure 1g**). Clinically, RT-qPCR showed that circEZH2 expression was significantly higher in BC cell lines, especially triple-negative BC (TNBC) lines, compared to normal breast epithelial cells (MCF-10A) (**Figure 1i**). Examination of clinical specimens revealed that circEZH2 was upregulated in BCLM samples relative to primary BC tissues (**Figure 1j**). Kaplan-Meier survival analysis indicated that elevated circEZH2 expression predicted poorer prognosis in BC patients (n = 115) (**Figure 1k**). FISH analysis further showed significantly higher circEZH2 expression in BCLM tissues compared to adjacent normal liver tissue (**Figure 1l**). Collectively, these findings indicate that circEZH2 is associated with BCLM and adverse clinical outcomes in BC.

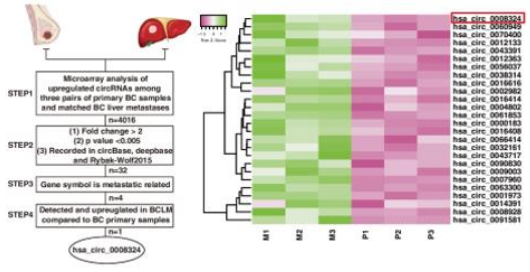

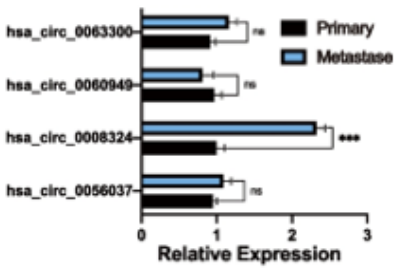

a)

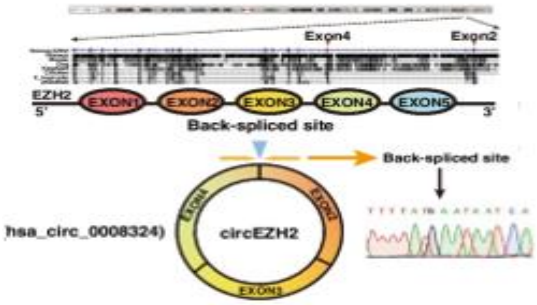
Exon4
Exon2
EZH2
EXON1
EXON2
EXON3
EXON4
EXON5
Back-spliced site
Back-spliced site
hsa_circ_0008324)
circEZH2
EXON4
EXON2
EXON3

b)

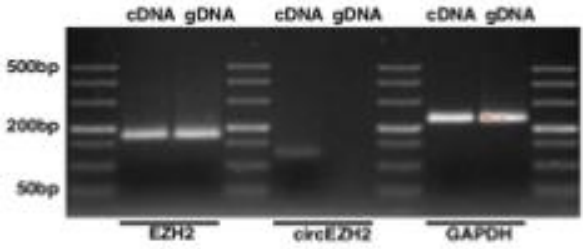
cDNA gDNA
cDNA gDNA
cDNA gDNA
500bp
200bp
50bp
EZH2
circEZH2
GAPDH

c)

d)

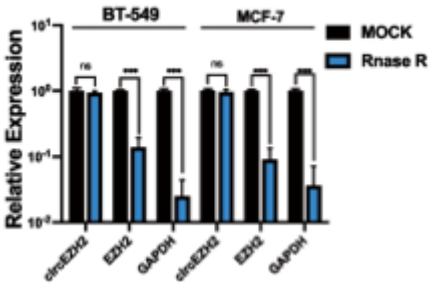
BT-549
MCF-7
MOCK
Rnase R
Relative Expression
circEZH2
EZH2
GAPDH
circEZH2
EZH2
GAPDH

e)

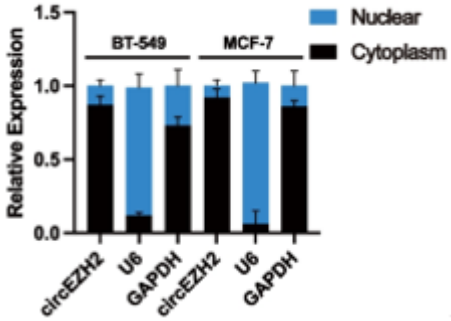
Nuclear
Cytoplasm
BT-549
MCF-7
Relative Expression
circEZH2
U6
GAPDH
circEZH2
U6
GAPDH

f)

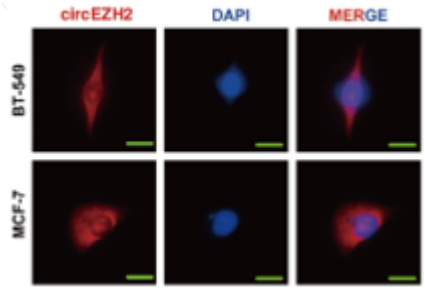
circEZH2
DAPI
MERGE
BT-549
MCF-7

g)

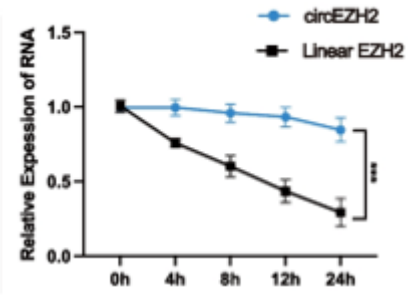
circEZH2
Linear EZH2
Relative Expression of RNA
0h
4h
8h
12h
24h

h)

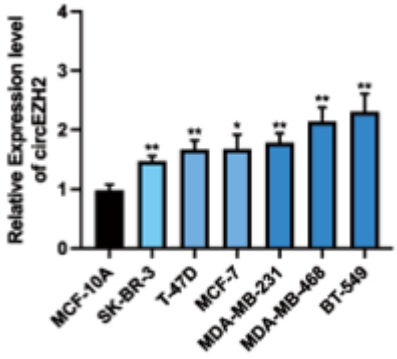
Relative Expression level of circEZH2
MCF-10A
SK-BR-3
T-47D
MCF-7
MDA-MB-231
MDA-MB-468
BT-549

i)

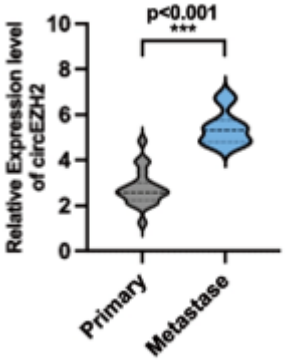
p<0.001
***
Relative Expression level of circEZH2
Primary
Metastase

j)

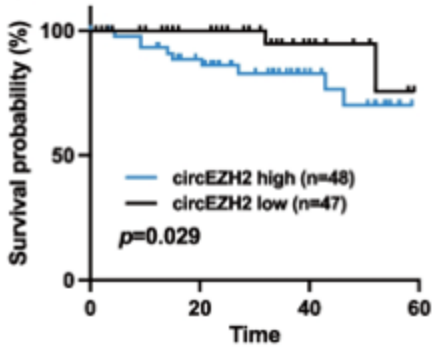

k)

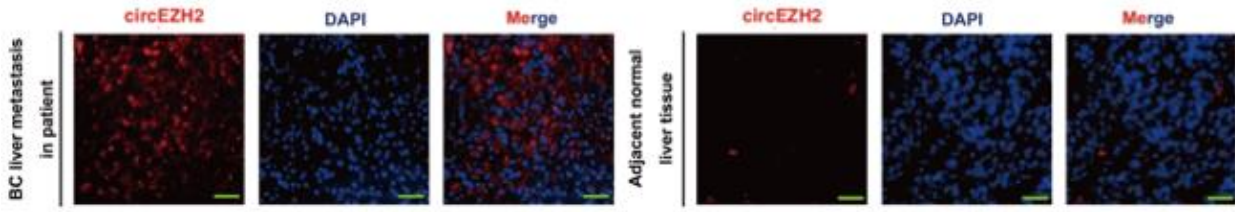

l)

Figure 1. Identification and characterization of circEZH2 in BC.

a Left, schematic workflow illustrating the selection criteria for circRNAs upregulated in BCLM; Right, heatmap showing 32 circRNAs chosen based on step 2 criteria, with hsa_circ_0008324 highlighted in a red box.
b RT-qPCR analysis was conducted to validate the expression of four candidate circRNAs in BC liver metastases and primary tumors.
c Top, sequence conservation of the three exons of circEZH2 across different species according to NCBI; Bottom, circEZH2 structure and Sanger sequencing confirming the back-splice junction.
d PCR amplification of circEZH2 using divergent and convergent primers in cDNA and gDNA, with linear EZH2 and GAPDH as controls.
e Following RNase R treatment, RT-qPCR was applied to assess changes in circEZH2 and linear EZH2 levels.
f Nuclear-cytoplasmic fractionation assays were performed to determine the subcellular distribution of circEZH2.
g FISH assays confirmed predominant cytoplasmic localization of circEZH2 (Scale bar, 20 μm).
h Actinomycin D treatment (4, 8, 12, 24 h) was used to examine the stability of circEZH2 and linear EZH2.
i RT-qPCR quantified circEZH2 expression across different BC cell lines.
j Expression levels of circEZH2 were verified in primary BC tissues (n = 20) and liver metastases (n = 11) via RT-qPCR; statistical significance was assessed by unpaired Student's t-test.
k Kaplan-Meier survival analysis of BC patients (n = 115) was conducted using log-rank tests.
l FISH analysis in BCLM samples demonstrated marked overexpression of circEZH2 (magnification: X4, scale bar 200 μm; X20, scale bar 50 μm). Data are presented as mean ± SD; experiments were repeated at least three times. ns: not significant; * $p < 0.05$; ** $p < 0.01$; *** $p < 0.001$.

CircEZH2 enhances the proliferation and metastasis of BC cells in vitro

To investigate the functional role of circEZH2, a circEZH2 overexpression plasmid and two siRNAs targeting circEZH2 were constructed (**Figure 2a**). Transfection efficiently upregulated or silenced circEZH2 in BC cell lines, while linear EZH2 levels remained unchanged (**Figures 2b and 1a**).

Cell proliferation was evaluated using EdU incorporation, CCK-8, and colony formation assays. Overexpression of circEZH2 significantly promoted BC cell proliferation, whereas knockdown of circEZH2 markedly reduced viability (**Figures 2c–2e**). Migration and invasion were assessed by transwell assays and wound-healing experiments. Suppression of circEZH2 impaired migratory and invasive abilities, while

circEZH2 overexpression had the opposite effect (**Figures 2f–2g**). These results demonstrate that circEZH2 promotes oncogenic growth and metastatic potential of BC cells in vitro.

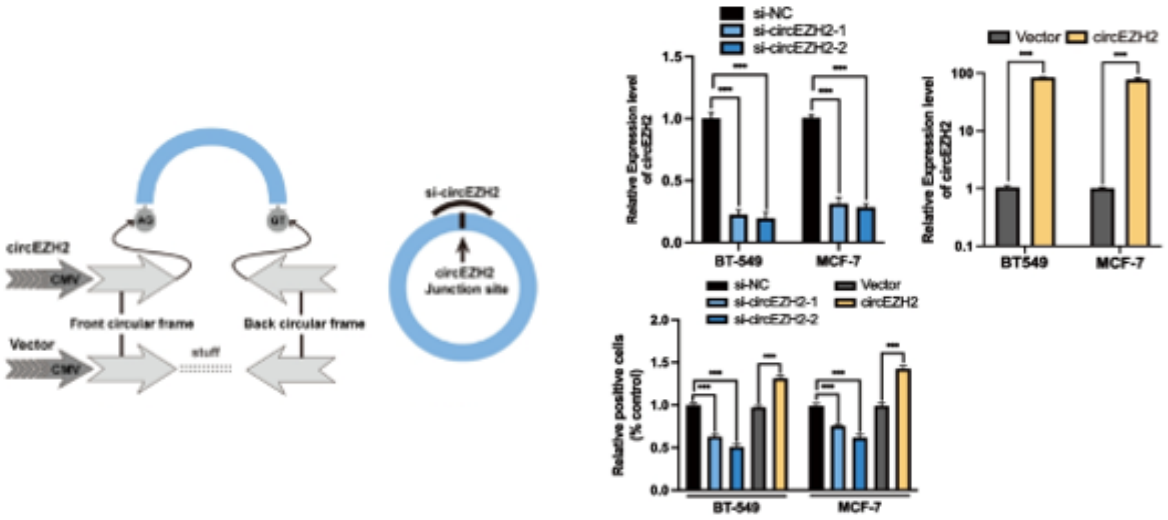

a) b)

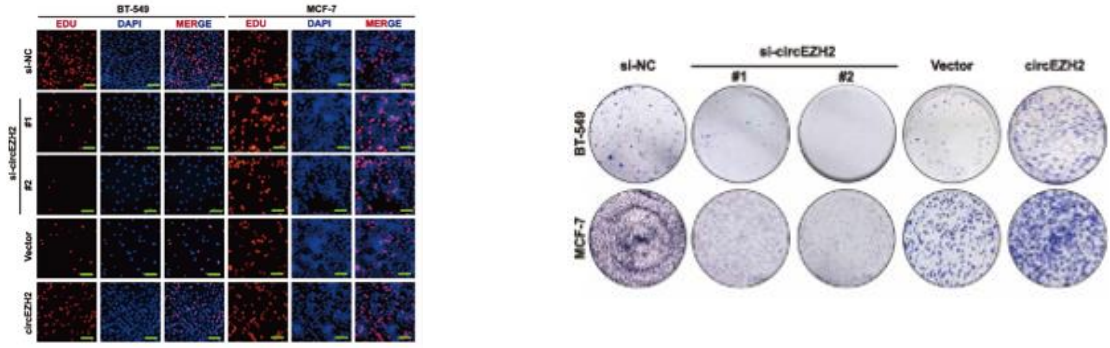

c) d)

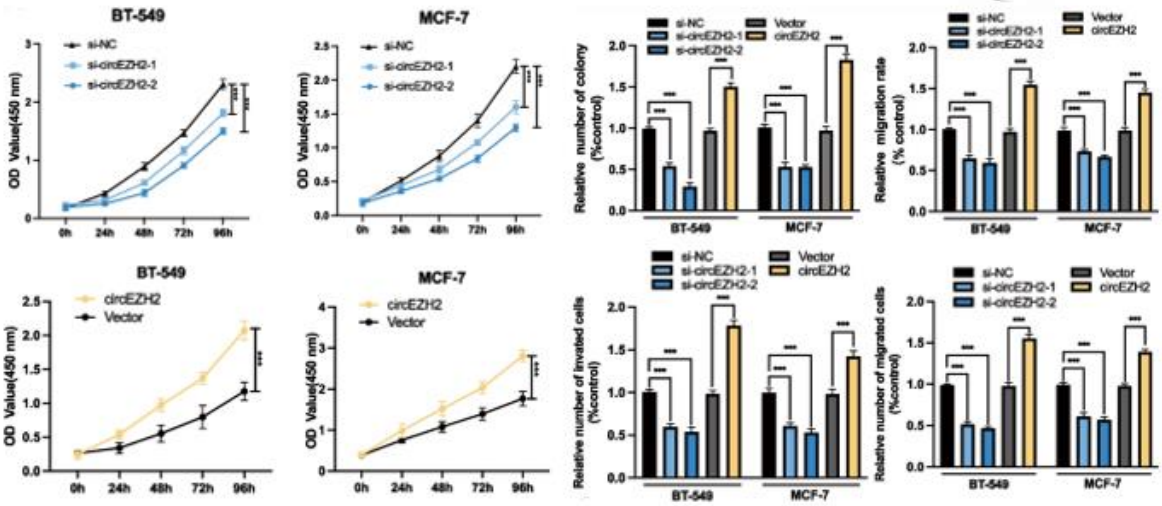

e)

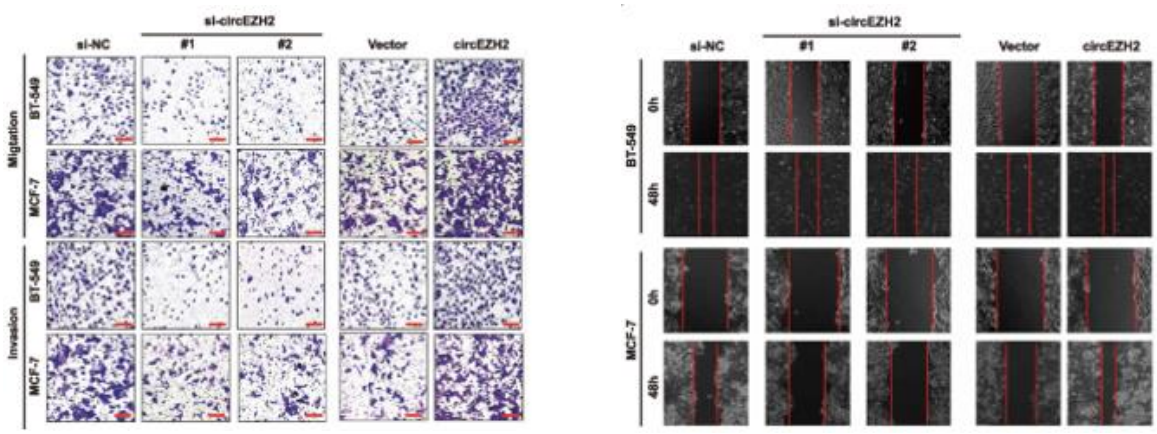

f) g)

Figure 2. CircEZH2 enhances proliferation, migration, and invasion of BC cells in vitro

a Schematic diagram depicting circEZH2 overexpression via plasmid and knockdown using siRNAs. **b** RT-qPCR confirmed the efficiency of circEZH2 overexpression or silencing. **c–e** EdU (scale bar, 50 μm), colony formation, and CCK-8 assays were employed to assess BC cell proliferation. **f–g** Migration and invasion were evaluated through transwell assays (scale bar, 100 μm) and wound-healing assays (scale bar, 200 μm). Data are presented as mean ± SD from at least three independent experiments, *p < 0.05; **p < 0.01; ***p < 0.001.

CircEZH2 promotes tumor growth and hepatic metastasis in vivo

To examine the role of circEZH2 in BC tumorigenesis, human BC xenograft models were established by subcutaneous injection of MCF-7 and BT-549 cells stably overexpressing circEZH2 or their corresponding controls into BALB/C nude mice. Tumors derived from circEZH2-overexpressing cells were significantly larger and heavier than control tumors (**Figures 3a–3c**).

To evaluate liver metastasis, stable circEZH2-overexpressing MCF-7 and BT-549 cells and control cells were injected into the inferior hemi-spleen of mice. CircEZH2-overexpressing mice exhibited higher luciferase signals and more hepatic nodules compared to controls (**Figures 3d–3g**). These in vivo findings are consistent with in vitro results, indicating that circEZH2 enhances BC tumorigenesis and liver metastatic potential.

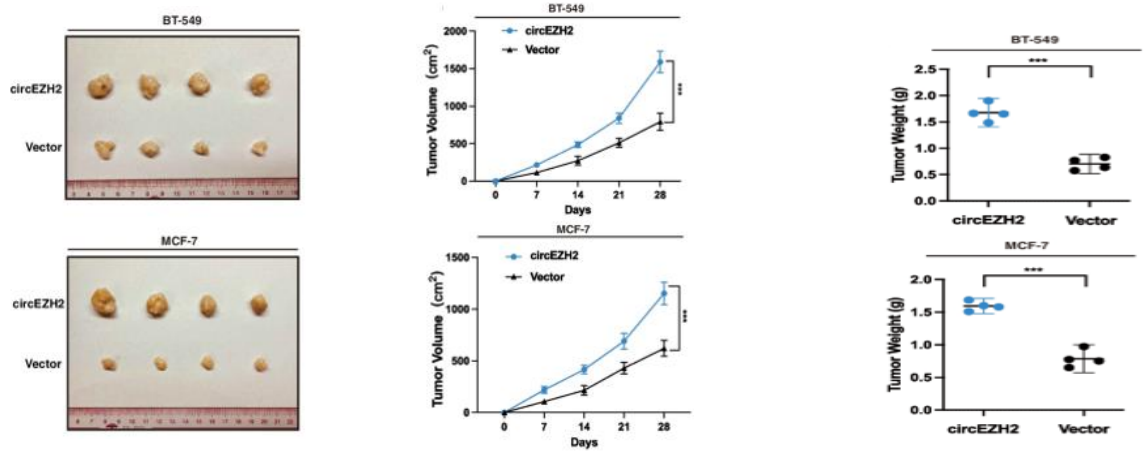

a) b) c)

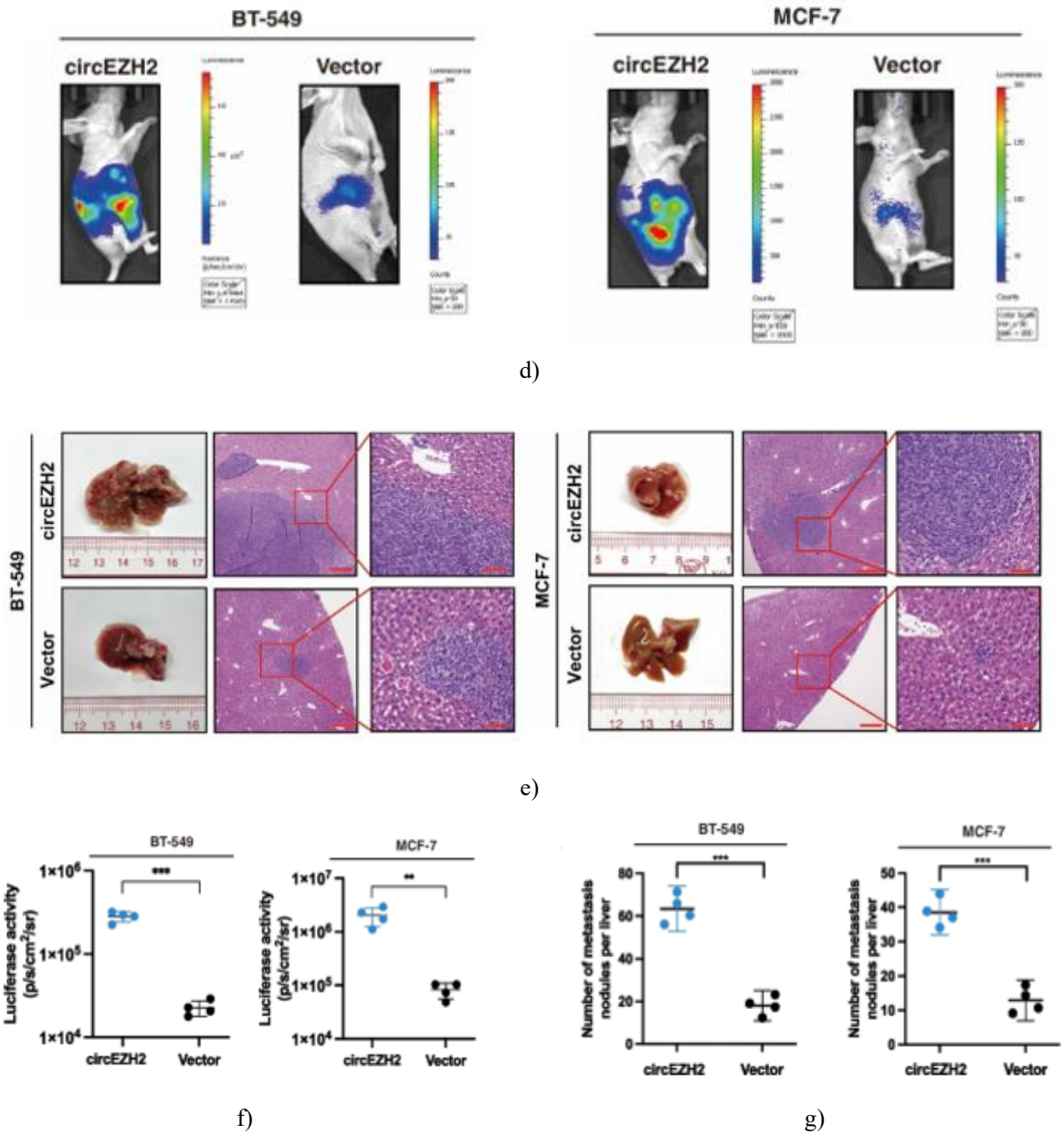

Figure 3. CircEZH2 promotes BC tumor growth and hepatic metastasis in vivo. **a** Images of xenograft tumors in circEZH2-overexpression and control groups (n = 4). **b** Growth curves of xenograft tumors. **c** Tumor weights measured and analyzed. **d–e** Inferior hemi-spleen injection models were monitored via IVIS to evaluate circEZH2-induced liver metastasis. **f–g** Liver metastatic sites increased in circEZH2-overexpressing mice, with H&E staining marking metastases (arrows; magnification: X4 scale bar 200 μm; X20 scale bar 40 μm). Data are presented as mean ± SD from at least three independent experiments, **p < 0.01; ***p < 0.001.

FUS facilitates circEZH2 back-splicing

Using circInteractome [19], four potential RNA-binding proteins (RBPs) were predicted in intronic regions flanking pre-EZH2 (the precursor of circEZH2): EIF4A3, FUS, PTBP1, and U2AF65. siRNAs targeting each candidate were transfected into BT-549 cells, revealing that FUS most strongly influenced circEZH2 expression (**Figures 4a–4b**).

Analysis of the TCGA database showed that FUS transcripts were upregulated in stage 1–4 breast cancer compared to normal tissue and across luminal, HER2+, and TNBC subtypes, suggesting FUS may play a key role

in BC initiation (**Figure 4c**). RT-qPCR of SYSUCC BC samples revealed a positive correlation between FUS and circEZH2 expression (**Figure 4d**), which was further confirmed in BC cells after modulating FUS levels (**Figure 4e**).

We hypothesized that FUS promotes circEZH2 back-splicing by binding to the 3′-flanking intron of pre-EZH2. A biotinylated pre-EZH2 probe encompassing 1250 bp downstream of exon 4 was used in RNA pull-down assays, confirming enrichment of FUS relative to control (**Figure 4f**). Five truncated biotinylated probes were generated to localize the FUS-binding site, identifying the second truncated probe as the primary binding region (**Figures 4g–4h**). RIP assays further validated the interaction between FUS protein and pre-EZH2 RNA (**Figure 4i**).

To confirm FUS's essential role in circEZH2 back-splicing, pc-HA-EZH2 vectors were designed: wild-type (WT) and a mutant (MT) with disrupted FUS-binding sites. HEK-293T cells co-transfected with FUS siRNA and WT or MT vectors showed that either FUS knockdown or mutation of the binding site significantly reduced circEZH2 back-splicing efficiency (**Figures 4j–4k**). Collectively, these data indicate that FUS promotes circEZH2 formation by binding to the 3′-flanking intron of pre-EZH2.

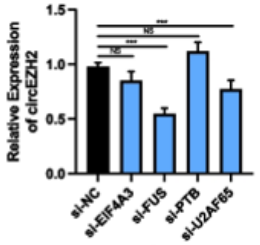

a)

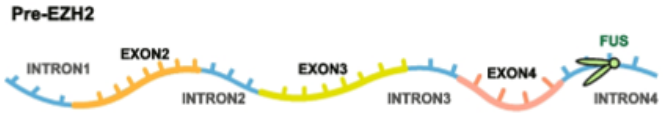

b)

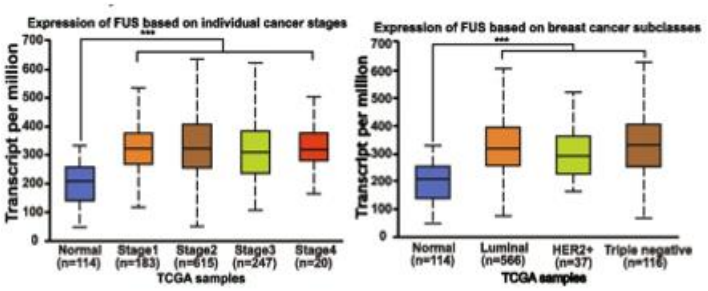

c)

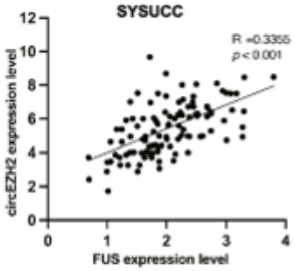

d)

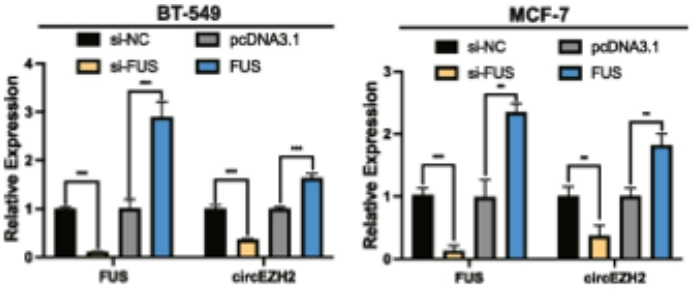

e)

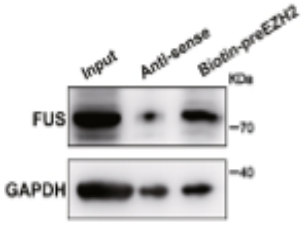

f)

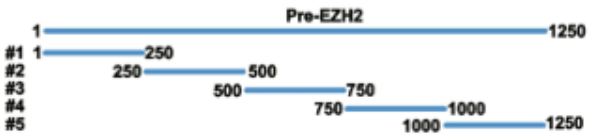

g)

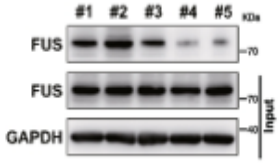

h)

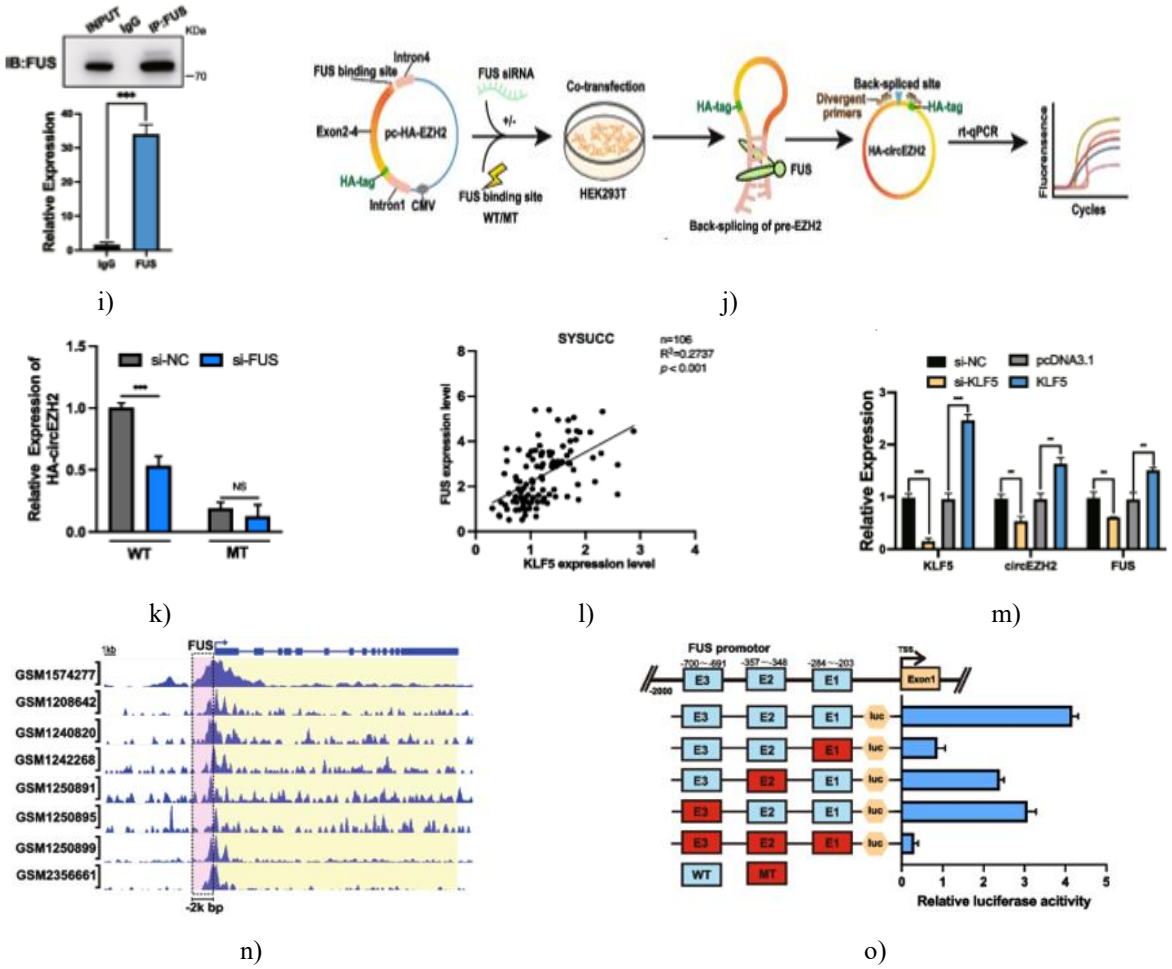

Figure 4. FUS facilitates circEZH2 back-splicing and KLF5 transcriptionally activates FUS

a RT-qPCR analysis of circEZH2 expression after transfection with siRNAs targeting EIF4A3, FUS, PTBP1, U2AF65, or control. **b** Schematic representation showing FUS binding to the downstream intron 4 region of pre-EZH2. **c** TCGA database analysis of FUS expression across BRCA stages and subtypes. **d** RT-qPCR of SYSUCC BC samples revealed a positive correlation between circEZH2 and FUS mRNA levels (Spearman correlation). **e** Alteration of FUS levels in BC cells modulated circEZH2 expression as determined by RT-qPCR. **f** Western blot analysis of RNA pull-down using biotinylated pre-EZH2 probe confirmed FUS enrichment. **g** Diagram showing the design of five truncated biotinylated pre-EZH2 probes. **h** RNA pull-down with truncated probes followed by western blot identified the second truncated probe as the main FUS-binding region. **i** RIP assays in BT-549 cells using anti-FUS and anti-IgG antibodies verified interaction between FUS and pre-EZH2. **j** Flowchart illustrating the pc-HA-EZH2 vector design: HA tag inserted at the 5′ end of exon 2 of EZH2; FUS-binding site mutated in the MT vector. WT or MT vectors were transfected into HEK293T cells with or without FUS knockdown, and circEZH2 back-splicing efficiency was measured using divergent primers across the HA tag, with linear HA-EZH2 as a reference. **k** RT-qPCR quantification of circEZH2 back-splicing in WT and MT groups. **l** Spearman correlation analysis of KLF5 and FUS expression in SYSUCC BC tissues. **m** RT-qPCR revealed changes in KLF5, circEZH2, and FUS levels after KLF5 modulation. **n** ChIP-seq datasets indicated KLF5 binding peaks within 2 kb upstream of the FUS promoter. **o** JASPAR predicted three potential KLF5 binding sites in the FUS promoter; dual-luciferase assays using wild-type and mutated promoters validated the regulatory interaction. Data are mean ± SD; all experiments repeated ≥3 times; ns, not significant; **p < 0.01, ***p < 0.001.

CircEZH2 functions as a miR-217-5p sponge

To explore the mechanism of circEZH2, bioinformatic analyses using miRanda [20] and circInteractome [19] identified five potential miRNAs binding circEZH2: miR-217, miR-554, miR-924, and miR-556 (**Figure 5a**). RNA pull-down assays revealed that miR-217-5p was the most enriched among candidates **Figures 5b–5c**). TCGA analysis of 1,165 paired tissues showed lower miR-217-5p expression in BRCA tissues compared to normal breast, suggesting a tumor-suppressive role (**Figure 1c**). To validate circEZH2–miR-217-5p interaction, dual-luciferase vectors containing either wild-type circEZH2 sequences or mutant sequences disrupting the predicted binding site were constructed (**Figure 5d**). miR-217-5p inhibitors significantly increased luciferase activity, while mimics reduced it; no effect was observed with the mutant vector (**Figure 5e**), confirming direct binding.

Rescue experiments were performed in BC cells by co-transfecting miR-217-5p mimics or inhibitors with circEZH2 overexpression or si-circEZH2, respectively. Functional assays—including EdU, CCK-8, colony formation, transwell migration, and wound-healing—showed that miR-217-5p mimics reversed the proliferative and invasive effects of circEZH2 overexpression, while miR-217-5p inhibition counteracted the effects of circEZH2 knockdown (**Figures 5f–5j**). These results demonstrate that circEZH2 sequesters miR-217-5p, suppressing its tumor-suppressive function and promoting BC progression.

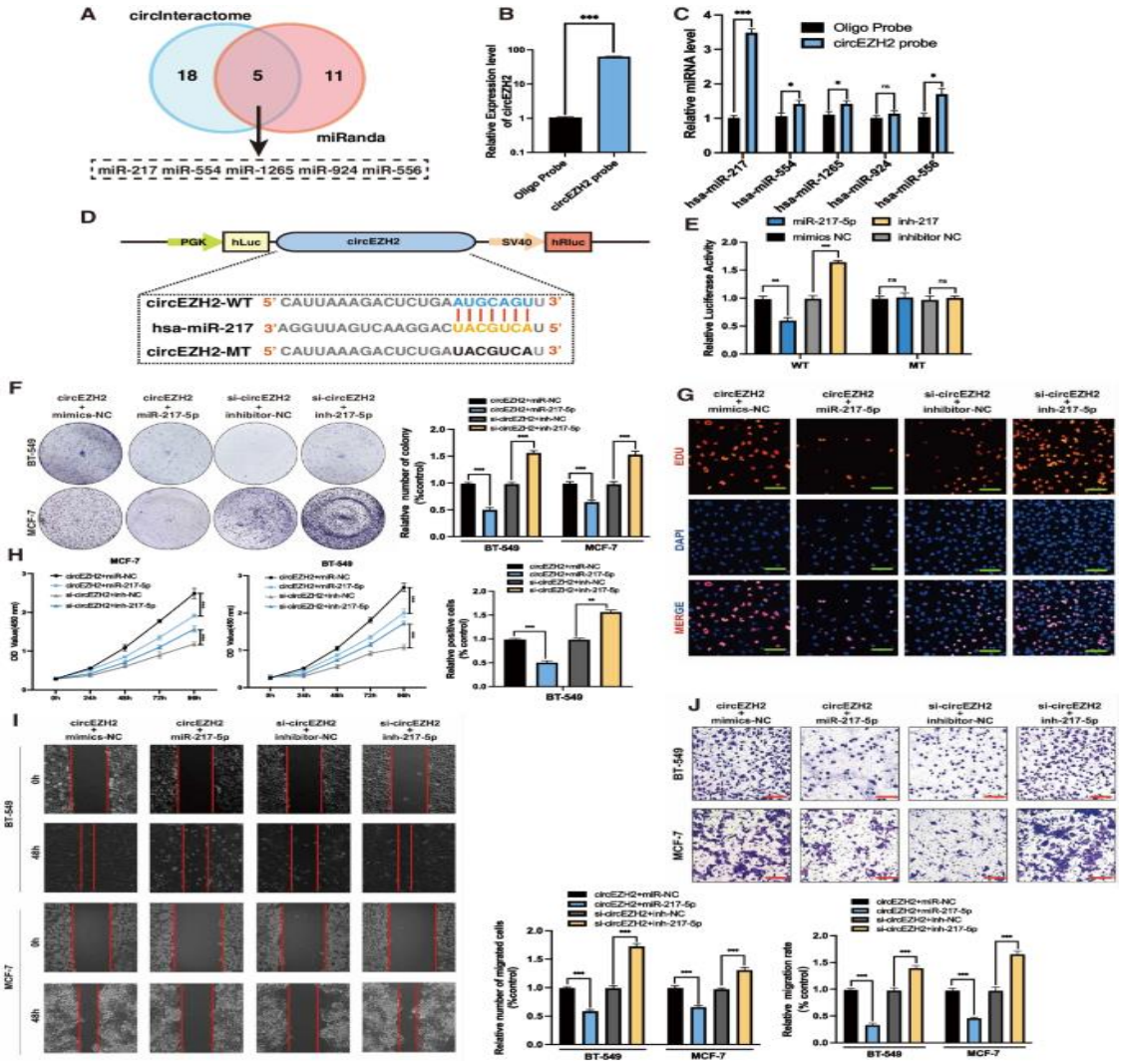

Figure 5. CircEZH2 sponges miR-217-5p. **a** Venn diagram showing overlapping miRNAs predicted by CircInteractome and miRanda. **b–c** RNA pull-down confirmed hsa-miR-217-5p as the most enriched; biotin-

labeled miR-217-5p efficiently captured circEZH2. **d–e** Dual-luciferase assays using WT and MT circEZH2 plasmids co-transfected with miR-217-5p mimics or inhibitors, assessing relative luciferase activity. **f–h** Co-transfection in BC cells assessed proliferation using colony formation, EdU (scale bar, 50 μm), and CCK-8 assays. **i–j** Migration assays including transwell (scale bar, 100 μm) and wound-healing (scale bar, 200 μm) validated metastatic potential. Data are mean ± SD; experiments repeated ≥3 times; ns, not significant; **p < 0.01, ***p < 0.001.

KLF5 is a direct target of the circEZH2/miR-217-5p axis to promote metastasis

To investigate the mechanistic role of the circEZH2/miR-217-5p axis, we performed bioinformatic analysis using miRMap [21], microT [22], miRDB [23], and TargetScan [24] with defined binding score thresholds, identifying 27 genes common to all four databases. A refined filtering strategy was then applied: (1) KM-plot analysis in TCGA to select genes associated with poor BC prognosis; (2) RT-qPCR to identify genes downregulated by miR-217-5p mimics; (3) literature review to select KLF5 as a final candidate, given its established role as an oncogenic transcription factor in BC and association with poor prognosis [25, 26] (**Figure 6a**).

RNA pull-down using a biotin-labeled miR-217-5p probe confirmed enrichment of KLF5 3′ untranslated region (UTR) compared with control (**Figure 6b**). RT-qPCR analysis of SYSUCC BC specimens revealed a negative correlation between KLF5 and miR-217-5p (**Figure 6d**), while dual-luciferase assays previously validated post-transcriptional regulation of KLF5 by miR-217-5p [18].

Next, the relationship between circEZH2 and KLF5 was assessed. RT-qPCR of clinical BC samples showed a positive correlation between circEZH2 and KLF5 (**Figure 6e**). Overexpression or knockdown of circEZH2 in BC cells resulted in corresponding increases or decreases in KLF5 mRNA and protein levels as detected by RT-qPCR and western blot (**Figures 1e–1f**). Rescue experiments with miR-217-5p inhibitor or mimics demonstrated that miR-217-5p inhibition restored KLF5 levels in circEZH2-knockdown cells, whereas miR-217-5p mimics attenuated KLF5 upregulation in circEZH2-overexpressing cells **(Figures 6f–6g and 1i)**. These findings confirmed that KLF5 is a downstream target of the circEZH2/miR-217-5p axis.

TCGA KM-Plotter analysis indicated that high KLF5 expression was associated with worse relapse-free survival in BC patients (**Figure 1h**) and that KLF5 is enriched in basal-like BC subtype according to BC GenExMiner [27] (**Figure 6c**). Immunofluorescence of BCLM patient samples revealed markedly higher KLF5 expression in liver metastases compared with normal liver tissue (**Figure 1e**). Collectively, these data indicate that KLF5 is linked to poor prognosis and liver metastasis in BC.

Considering BC heterogeneity and multi-organ metastasis, xenograft-induced metastasis models were established using BT-549 cells in BALB/C nude mice. Cells were injected into the mammary pad (n = 5) to promote tumor growth, and tumors were surgically removed when the short diameter reached 2 cm. Eight weeks later, metastases were observed: 2 mice with liver and brain metastases and 3 mice with lung metastases (**Figure 6h**). Protein and RNA extracted from metastatic tissues revealed that circEZH2 was upregulated in liver, brain, and lung metastases, with the highest expression in liver metastases (**Figure 6i**). KLF5 protein was elevated in liver and brain metastases, while FUS was increased in liver, brain, and lung metastases relative to parental cells (**Figures 6j–6k**). KLF5 and FUS protein levels showed a positive correlation consistent with clinical observations (**Figure 6l**). These results suggest that the FUS/circEZH2/KLF5 axis may contribute to multi-organ metastasis.

To specifically evaluate circEZH2 and KLF5 regulation in liver metastasis in vivo, doxycycline-inducible KLF5-shRNA cell lines were generated under circEZH2 overexpression using the pLKO-Tet-On-shRNA plasmid (Addgene #98398). Doxycycline treatment efficiently reduced KLF5 protein levels and concomitantly decreased FUS expression (**Figure 6m**). Transwell migration assays and liver metastasis models demonstrated that KLF5 knockdown significantly impaired circEZH2-induced migration in vitro and reduced liver metastatic nodules and luciferase activity in vivo (**Figures 6n–6o**). Immunohistochemistry confirmed reduced FUS expression in hepatic metastases of KLF5-knockdown mice (**Figure 6p**).

These findings collectively demonstrate that KLF5 is essential for circEZH2-mediated liver metastasis and functions upstream of FUS, regulating its expression and contributing to BC progression both in vitro and in vivo.

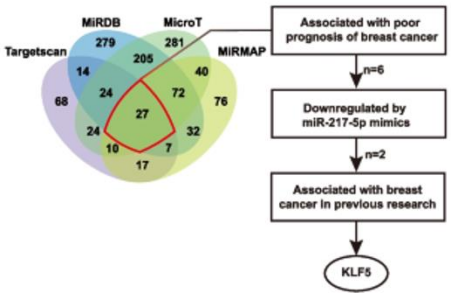
MiRDB
MicroT
Targetscan
MiRMAP
279
281
205
14
40
68
24
72
76
27
24
32
10
7
17
Associated with poor prognosis of breast cancer
n=6
Downregulated by miR-217-5p mimics
n=2
Associated with breast cancer in previous research
KLF5

a)

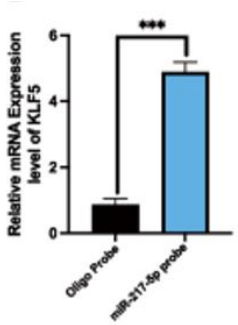
***
Relative mRNA Expression level of KLF5
Oligo Probe
miR-217-5p probe

b)

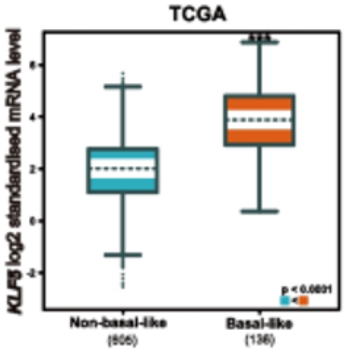
TCGA
KLF5 log2 standardised mRNA level
Non-basal-like
(806)
Basal-like
(136)

c)

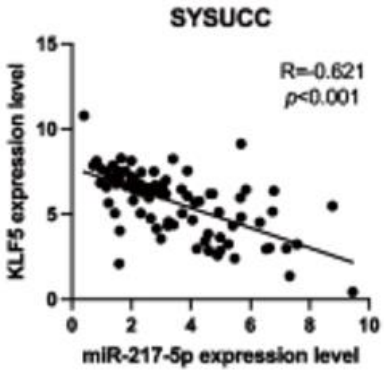
SYSUCC
R=-0.621
p<0.001
KLF5 expression level
miR-217-5p expression level

d)

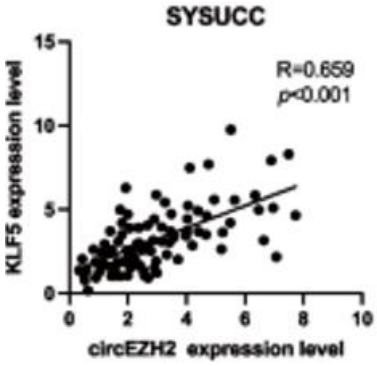
SYSUCC
R=0.659
p<0.001
KLF5 expression level
circEZH2 expression level

e)

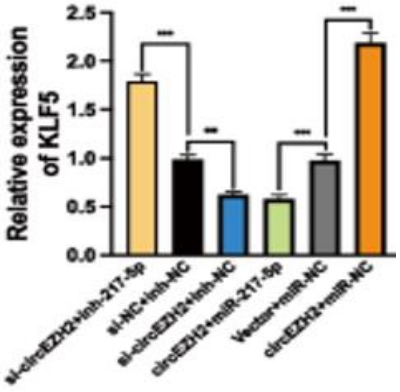
Relative expression of KLF5
si-circEZH2+inh-217-5p
si-NC+inh-NC
si-circEZH2+inh-NC
circEZH2+miR-217-5p
Vector+miR-NC
circEZH2+miR-NC

f)

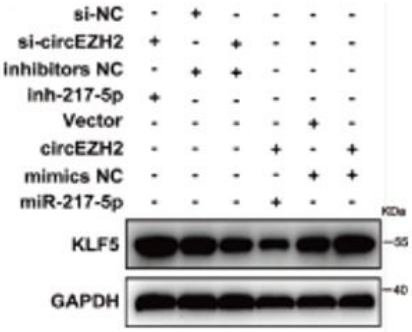
si-NC
si-circEZH2
inhibitors NC
inh-217-5p
Vector
circEZH2
mimics NC
miR-217-5p
KDa
KLF5
55
GAPDH
40

g)

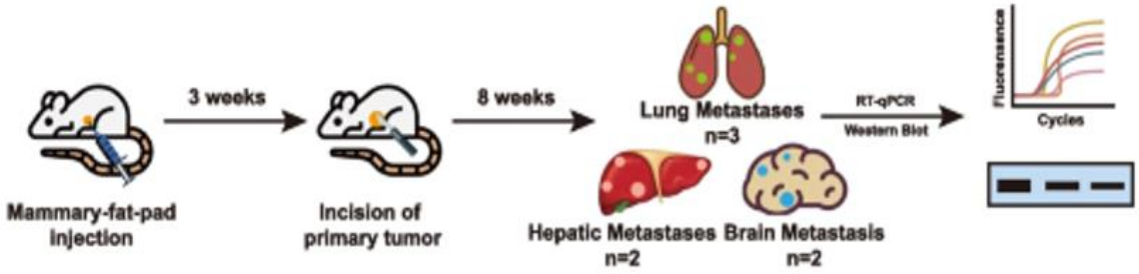
3 weeks
8 weeks
Lung Metastases
n=3
RT-qPCR
Western Blot
Fluorescence
Cycles
Mammary-fat-pad injection
Incision of primary tumor
Hepatic Metastases
n=2
Brain Metastasis
n=2

h)

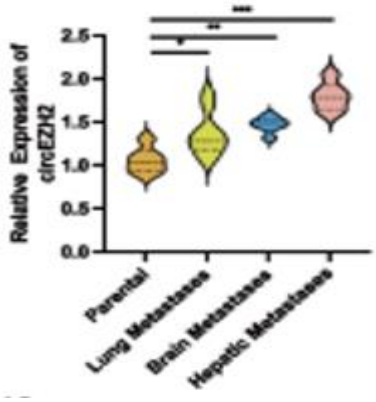
Relative Expression of circEZH2
Parental
Lung Metastases
Brain Metastases
Hepatic Metastases

i)

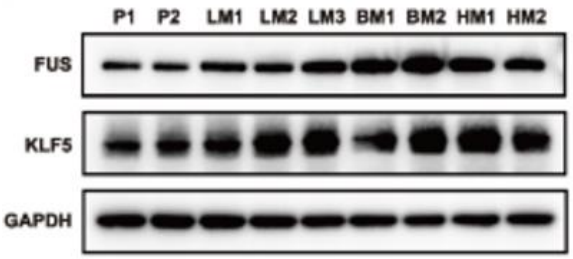
P1 P2 LM1 LM2 LM3 BM1 BM2 HM1 HM2
FUS
KLF5
GAPDH

j)

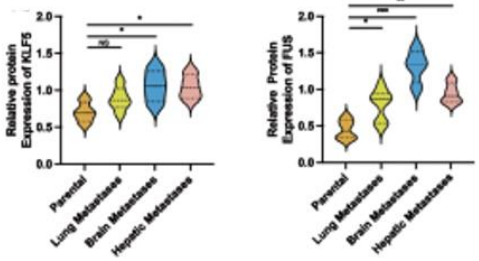
Relative protein Expression of KLF5
Relative Protein Expression of FUS
Parental
Lung Metastases
Brain Metastases
Hepatic Metastases

k)

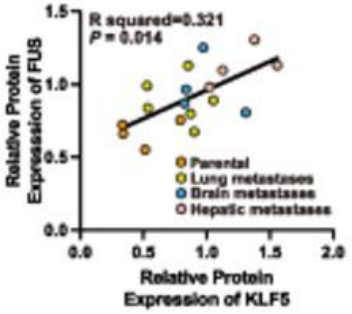
R squared=0.321
P = 0.014
Relative Protein Expression of FUS
Relative Protein Expression of KLF5
Parental
Lung metastases
Brain metastases
Hepatic metastases

l)

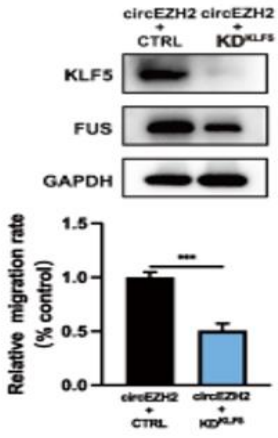
circEZH2 + CTRL
circEZH2 + KD^KLF5
KLF5
FUS
GAPDH
Relative migration rate (% control)

m)

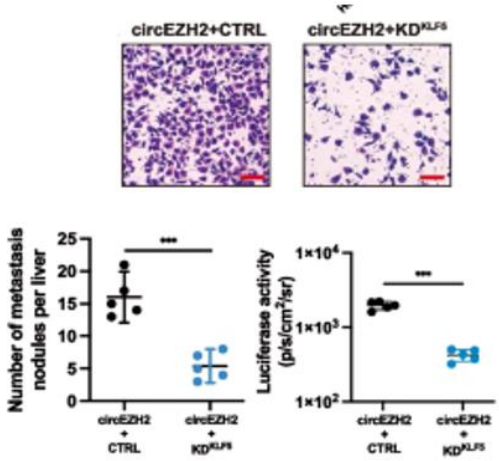
circEZH2+CTRL
circEZH2+KD^KLF5
Number of metastasis nodules per liver
Luciferase activity (p/s/cm²/sr)

n)

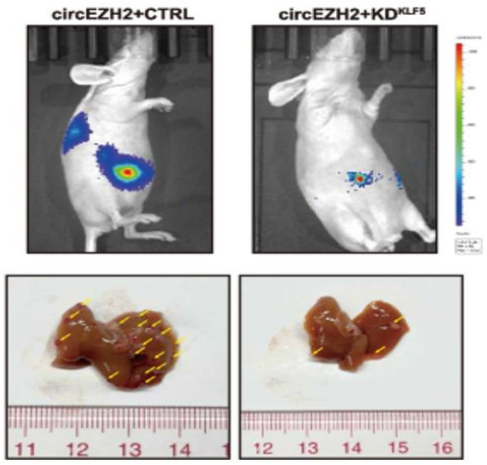

o)

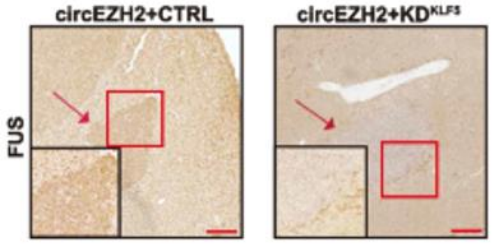

p)

Figure 6. KLF5 is a direct target of miR-217-5p

a Left, Venn diagram illustrating potential miR-217-5p target genes identified by miRDB, microT, TargetScan, and miRMap. Right, flowchart outlining stepwise filtering of candidate targets. **b** RNA pull-down using biotin-labeled miR-217-5p probe confirmed enrichment of KLF5 via RT-qPCR. **c** TCGA and BC-GenExMiner analyses revealed elevated KLF5 expression in the basal-like BC subtype. **d–e** Transcript analysis of SYSUCC clinical BC samples showed a negative correlation between miR-217-5p and KLF5 (right) and a positive correlation between circEZH2 and KLF5 (left) by Spearman correlation. **f–g** RT-qPCR and western blot analysis assessed KLF5 expression after co-transfection with siRNA, vector, mimics, or inhibitors as indicated. **h** Flowchart depicting establishment of xenograft-induced metastatic mice and analysis of multi-organ metastases by western blot and RT-qPCR. **i** RT-qPCR revealed circEZH2 expression patterns in metastases versus parental cells. **j–k** Western blot quantified FUS and KLF5 protein in metastases: P = parental; LM = lung; BM = brain; HM = liver. **l** Pearson correlation confirmed positive association between FUS and KLF5 in metastases. **m** Western blot validation of doxycycline-induced KLF5 knockdown in circEZH2-overexpressing cells. **n–o** Transwell migration and liver metastasis rescue assays demonstrated that KLF5 knockdown reduced circEZH2-induced migration; Transwell scale bar = 100 μm; liver metastases quantified by IVIS, nodules marked with yellow arrows. **p** IHC of FUS in hepatic metastases of KLF5-knockdown vs control groups (Low power: scale bar 100 μm; High power: scale bar 20 μm). Data are mean ± SD; experiments repeated ≥3 times; ns, not significant; *p < 0.05, **p < 0.01, ***p < 0.001.

KLF5 transcriptionally upregulates FUS and forms a positive circEZH2/KLF5/FUS feedback loop

Based on RT-qPCR analysis of clinical BC specimens from SYSUCC, FUS expression showed a significant positive correlation with KLF5 at the mRNA level (**Figure 4l**). Modulation of KLF5 expression, either upregulation or downregulation, led to corresponding increases or decreases in FUS and circEZH2 levels (**Figure 4m**), whereas linear EZH2 remained largely unchanged (**Figure 1b**), suggesting that KLF5 may transcriptionally regulate FUS. Subsequently, analysis of eight ChIP-seq datasets via the Cistrome data browser [28] revealed KLF5-enriched peaks within 2 kb upstream of the FUS promoter (**Figure. 4n**). Using JASPAR [29], three potential KLF5 binding sites were predicted on the FUS promoter. To investigate whether KLF5 directly activates FUS transcription, ChIP assays were conducted, showing that among the E1, E2, and E3 regions, E1 (−284 to −203) exhibited the strongest enrichment, consistent with prior findings (**Figure 1g**). To further validate KLF5's interaction with each site, promoter dual-luciferase assays were performed with individual site mutations; non-mutated constructs served as positive controls, while constructs with all sites mutated served as negative controls. Results indicated that the E1 region was critical for KLF5-mediated transcriptional activation, demonstrating that KLF5 enhances FUS transcription, thereby promoting circEZH2 expression via increased back-splicing

(**Figure 4o**). Collectively, these results support the establishment of a novel FUS/circEZH2/KLF5 positive feedback loop.

circEZH2 promotes EMT in BC via KLF5/CXCR4 axis

STARBASE analysis indicated that KLF5 positively correlates with CXCR4 RNA expression (**Figure 1j**). CXCR4 is associated with poor prognosis in BRCA and upregulated in primary tumors versus normal tissue. Analysis of seven ChIP-seq datasets via Cistrome revealed potential KLF5 binding peaks within 2 kb upstream of the CXCR4 TSS (**Figure 7a)**. JASPAR predicted three KLF5 binding sites (E1–E3); ChIP assays showed E2 as the most enriched site (**Figure 7b**). Dual-luciferase assays confirmed KLF5-dependent transcriptional activation of CXCR4, which was abolished in mutated promoters (**Figure 7c**).

Correlation analysis using STARBASE [30] demonstrated that KLF5 and CXCR4 expression positively associates with EMT markers; Spearman R values showed similar patterns for KLF5 and CXCR4 (**Figure 7d**). Both KLF5 and CXCR4 positively correlated with Vimentin and N-cadherin and negatively with E-cadherin (**Figure 7e**), suggesting that circEZH2 may drive EMT via KLF5-mediated CXCR4 activation. Western blot confirmed that circEZH2 overexpression enhanced EMT and CXCR4 expression, while KLF5 knockdown reversed these effects (**Figure 7f**). F-actin immunofluorescence showed reduced cytoskeletal remodeling upon circEZH2 or KLF5 knockdown.

CXCR4 inhibitor AMD3100 significantly suppressed proliferation and migration induced by circEZH2 or KLF5 overexpression, indicating CXCR4 is critical for the FUS/circEZH2/KLF5 feedback loop and may serve as a therapeutic target **(Figure 7h–7i**). IHC of hepatic metastases from nude mice showed increased KLF5, CXCR4, Vimentin, and N-cadherin and decreased E-cadherin in circEZH2-overexpressing tumors (**Figure 7j**). These findings demonstrate that the FUS/circEZH2/KLF5 axis promotes EMT via CXCR4, driving liver metastasis in BC (**Figure 8a**).

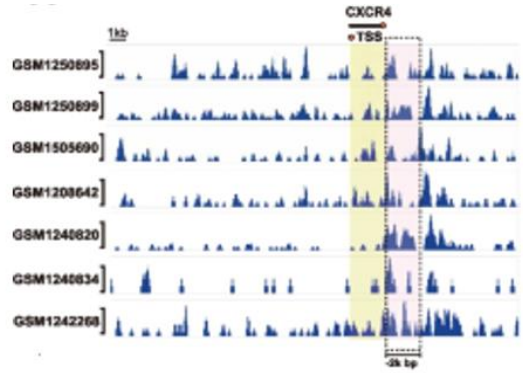

a)

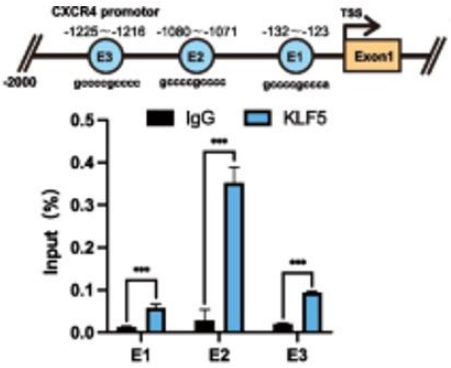

b)

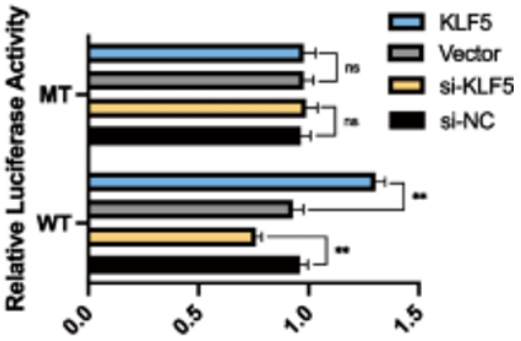

c)

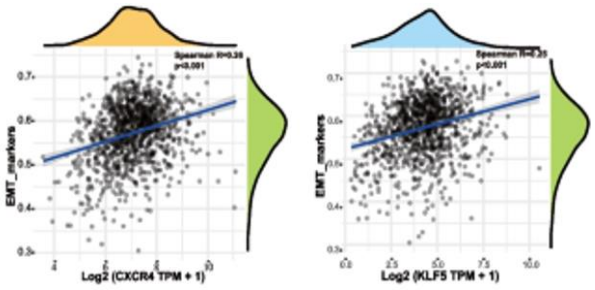

d)

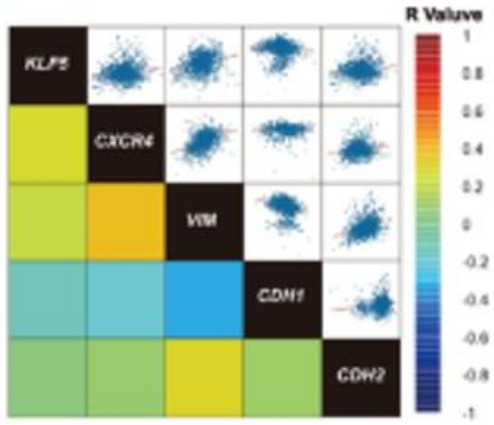
R Value
KLF5
CXCR4
VIM
CDH1
CDH2

e)

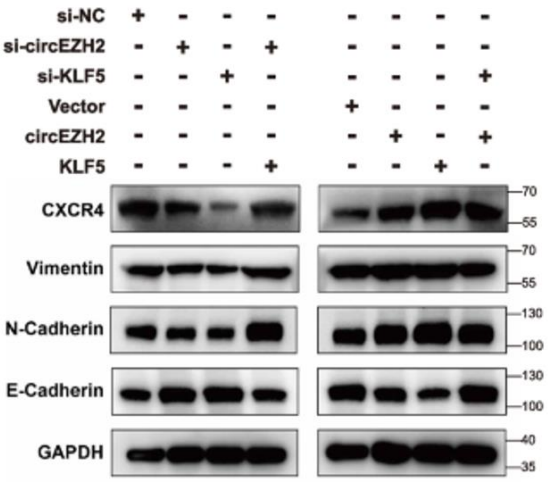
si-NC
si-circEZH2
si-KLF5
Vector
circEZH2
KLF5
CXCR4
Vimentin
N-Cadherin
E-Cadherin
GAPDH

f)

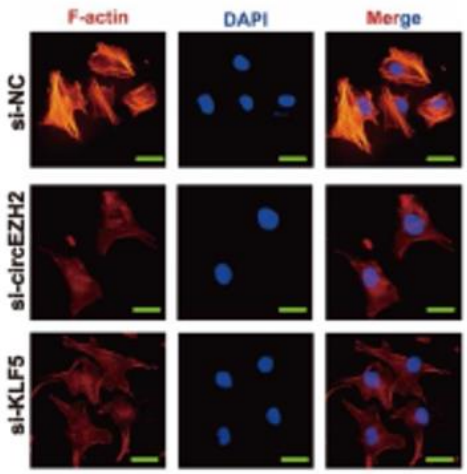
F-actin
DAPI
Merge
si-NC
si-circEZH2
si-KLF5

g)

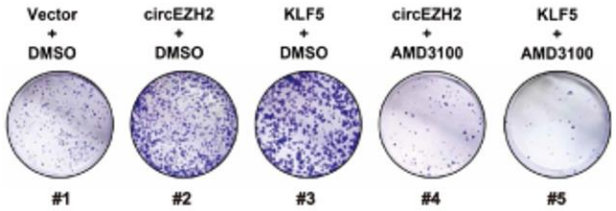
Vector + DMSO
circEZH2 + DMSO
KLF5 + DMSO
circEZH2 + AMD3100
KLF5 + AMD3100
#1
#2
#3
#4
#5

h)

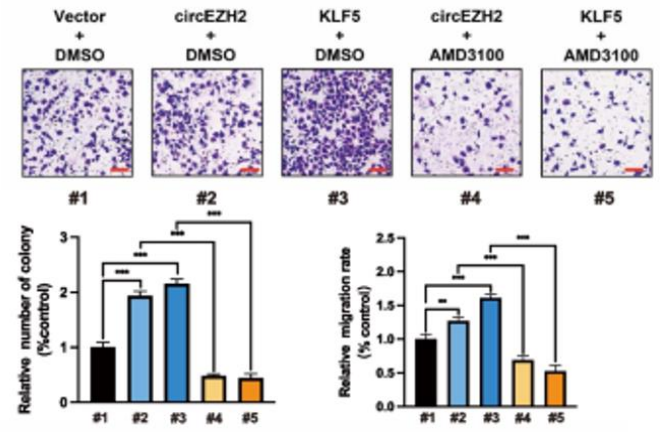
Vector + DMSO
circEZH2 + DMSO
KLF5 + DMSO
circEZH2 + AMD3100
KLF5 + AMD3100
#1
#2
#3
#4
#5
Relative number of colony (%control)
Relative migration rate (% control)

i)

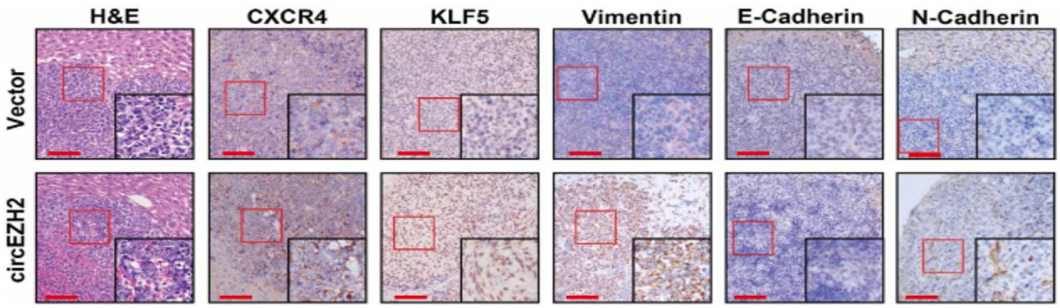

j)

Figure 7 FUS/circEZH2/KLF5 axis drives CXCR4-mediated EMT in BC

a Analysis of seven ChIP-seq datasets revealed KLF5 binding peaks within 2 kb upstream of the CXCR4 promoter. **b** Top, predicted KLF5 binding sites on the CXCR4 promoter according to JASPAR. **c** Dual-luciferase reporter assays were performed in wild-type and E2-mutated CXCR4 promoter constructs. **d** TCGA GSVA analysis demonstrated a positive correlation between KLF5 or CXCR4 and EMT marker expression. **e** Regression correlation heatmap from STARBASE showed relationships among KLF5, CXCR4, VIM, CDH1, and CDH2 transcripts. **f** Western blot analyzed CXCR4, Vimentin, N-cadherin, and E-cadherin levels following indicated siRNA or vector treatments. **g** Immunofluorescence (IF) revealed a marked reduction of F-actin after circEZH2 or KLF5 knockdown. **h–i** CXCR4-rescue experiments included colony formation and transwell migration assays under indicated vectors or drugs (scale bar 100 μm). **j** IHC in circEZH2-overexpressing BCLM nude mice versus controls with specific antibodies (low power: 100 μm; high power: 20 μm). Data are mean ± SD; experiments repeated ≥3 times; ns, not significant; *P < 0.05, **P < 0.01, ***P < 0.001.

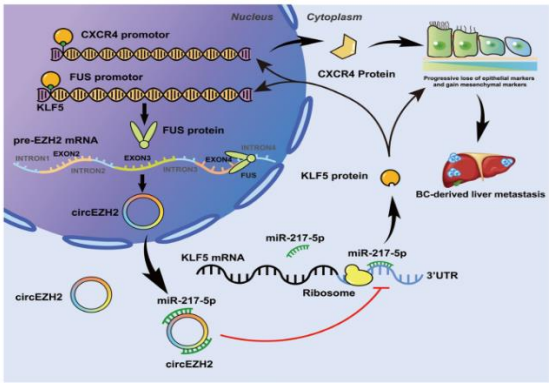

Figure 8a Schematic illustrating the biological mechanism of the novel FUS/circEZH2/KLF5 positive feedback loop, promoting liver metastasis in breast cancer through EMT activation via CXCR4 upregulation.

Materials and Methods

Patient specimens

BCLM and primary BC tissues were collected from patients at Sun Yat-Sen University Cancer Center (SYSUCC, Guangzhou, China) and immediately preserved in RNAlater. All specimens were obtained with informed consent under IRB-approved protocols.

Cell lines and culture

Six human BC cell lines (MDA-MB-231, BT-549, T-47D, MCF-7, SKBR-3) and the normal breast epithelial line MCF-10A, along with HEK293T, were used (ATCC, Manassas, VA, USA). MDA-MB-231, SKBR-3, BT-549, T-47D, MCF-7, and HEK293T were maintained in DMEM (Gibco, USA), whereas MCF-10A was cultured in DMEM/F-12 (Gibco, NY, USA), supplemented with 10% FBS and 50 U/ml penicillin-streptomycin (Gibco, NY, USA). Cells were incubated at 37°C with 5% CO2 in a humidified incubator (Thermo Fisher Scientific, MA, USA).

Animal experiments

Female BALB/c nude mice (Vital River, Beijing, China) were housed under standard conditions at SYSUCC's Center for Experimental Animals. For xenograft tumor growth, 2 × 10^6 MCF-7 or BT-549 cells with stable circEZH2 overexpression or control were subcutaneously injected. Tumor volume was measured weekly using the formula: volume = length × width^2 / 2, and tumor weight was recorded at sacrifice after 4 weeks.

For liver metastasis models, 1 × 10^6 MCF-7 or BT-549 circEZH2-overexpressing cells expressing luciferase were injected into the spleen of 4–5-week-old female BALB/c mice, with corresponding controls. After 60 days, mice received 100 µl intraperitoneal D-luciferin (15 µg/µl) for bioluminescence imaging (Xenogen IVIS Lumina Series II) and data processed using Living Image 2.11 software. Livers were harvested for histopathological analysis post-sacrifice.

For xenograft-induced metastatic models, 2 × 10^6 BT-549 cells were injected into the mammary pad; tumors were surgically removed when the short diameter reached ~2 cm. After 8 weeks, metastases were visualized by bioluminescence, followed by organ harvesting for RNA and protein extraction. All procedures were approved by Sun Yat-Sen University Animal Care and Use Committee.

Statistical analysis

Statistical analyses were performed using SPSS 21.0 (IBM, IL, USA) and GraphPad Prism 9.1 (GraphPad, CA, USA). Comparisons between groups were assessed using Student's t-test. Spearman correlation coefficients quantified associations. Survival was evaluated by Kaplan-Meier analysis, with significance determined using the log-rank test.

Metastasis remains the leading cause of BC-related mortality worldwide [31]. The distinctive structural features and tissue-specific expression patterns of circRNAs have recently drawn significant attention in cancer research, offering potential biomarkers and therapeutic targets for BC [17, 32]. Therefore, elucidating the biological functions of circRNAs is essential to understand their role in BC metastasis. In this study, circEZH2 was identified through microarray analysis in three paired primary BC and BCLM samples due to its marked upregulation in BCLM and its association with poor prognosis. Functional assays further demonstrated that circEZH2 overexpression enhanced cell viability, invasion, and hepatic metastasis in vivo.

Multiple regulatory factors contribute to circRNA biogenesis from precursor mRNAs, including transcription factor Twist1 [33], splicing factor QKI [34], EIF4A3 [35, 36], and super-enhancer YY1 [37]. Recently, FUS has been recognized as a crucial mediator in circRNA synthesis [38, 39]. For instance, Han *et al.* reported that FUS facilitated colorectal cancer metastasis by back-splicing circLONP [40]. Our previous work confirmed that FUS binds the circROBO1 precursor to support its back-splicing [18]. In this study, we mutated the FUS binding site on pc-HA-EZH2 and modulated FUS expression, revealing that FUS markedly promotes circEZH2 back-splicing, a novel finding beyond our earlier research. Xenograft-induced metastatic mouse models further confirmed significant upregulation of FUS in hepatic, brain, and lung metastases, suggesting FUS may contribute to multi-organ metastasis. TCGA bioinformatic analysis showed FUS was consistently upregulated in BC tissues, though not stage-specific, implying a role in BC initiation. These observations indicate the necessity for further functional studies of FUS in oncogenesis.

The subcellular localization of circRNAs is critical to their function. Here, circEZH2 predominantly localized in the cytoplasm, and RNA pull-down assays demonstrated its interaction with hsa-miR-217-5p. Previous studies have identified miR-217-5p as a tumor suppressor in various cancers [41–44]. Our results revealed that circEZH2 modulates the oncogenic effects of BC by sponging miR-217-5p, as ectopic expression of miR-217-5p mitigated circEZH2-induced malignancy.

The transcription factor KLF5 is overexpressed in basal-like BC [45] and serves as a prognostic marker for poor outcomes [46, 47]. KLF5 promotes BC progression by regulating Slug [48], Cyclin D1 [49], Nanog [50], FGFBP1 [51], and TNFAIP2 [25], and has been implicated in metastasis in multiple cancers [26, 52, 53]. Bioinformatic analysis and RNA pull-down assays identified KLF5 as a direct target of miR-217-5p. CircEZH2 positively correlated with KLF5 expression at both mRNA and protein levels, which could be reversed by ectopic miR-217-5p. Xenograft-induced metastasis models confirmed KLF5 upregulation in hepatic and brain metastases and revealed a positive protein correlation between KLF5 and FUS. Doxycycline-inducible KLF5 knockdown cells demonstrated that reducing KLF5 significantly decreased circEZH2-driven metastasis in vitro and in vivo. KLF5 recognizes GCCCGCCC motifs in gene promoters; ChIP-seq and JASPAR predicted KLF5 binding sites on the FUS promoter. Subsequent ChIP and promoter-mutated dual-luciferase assays confirmed that KLF5 binds the E1 region of FUS promoter to enhance transcription, leading to increased circEZH2. This established the FUS/circEZH2/KLF5 positive feedback loop.

While primary BC can be treated with surgery and systemic chemotherapy, metastatic BC remains largely

untreatable due to the inefficacy of current therapies against disseminated tumor cells [54]. Metastasis is a multi-step cascade in which EMT is critical, driving detachment, migration, and invasion [55–57]. Zhang *et al*. reported that KLF5 maintains EMT and promotes bone metastasis and chemotherapy resistance in prostate cancer via CXCR4 upregulation [58]. CXCR4, a G-protein-coupled receptor for CXCL12, facilitates cellular migration, with liver, bone, lung, and lymph nodes providing high CXCL12 levels to support BC metastasis [59, 60]. CXCR4/CXCL12 signaling, along with phosphorylated mTOR, can induce EMT in metastatic BC [61]. Our analyses demonstrated that the FUS/circEZH2/KLF5 loop activates CXCR4 transcription, driving EMT. Activated hepatic stellate cells (aHSCs) secrete CXCL12, which can induce NK cell quiescence, promoting metastasis [62], highlighting the need to explore CXCR4 function within the hepatic metastatic niche. Prior work also showed KLF5 inhibits selective autophagy of Afadin, a skeletal protein interacting with claudin-2, essential for BCLM [18]. This study extends those findings by demonstrating that KLF5 drives BCLM via EMT, linking its role to the immune microenvironment.

Conclusion

We identified a novel circRNA, circEZH2, that promotes BC progression and liver metastasis. BCLM samples exhibited elevated circEZH2, correlating with poor prognosis. Mechanistically, circEZH2 sponges miR-217-5p, relieving post-transcriptional inhibition of KLF5 and enhancing CXCR4-driven EMT. FUS facilitates circEZH2 back-splicing and is transcriptionally upregulated by KLF5, establishing a FUS/circEZH2/KLF5/CXCR4 positive feedback loop. This axis represents a potential biomarker for BC metastasis and a therapeutic target for BC intervention.

Acknowledgments: Our thanks go to the Department of Breast Oncology, the Sun Yat-sen University Cancer Center, and the State Key Laboratory of Oncology in South China for offering clinical BC specimens with associated anonymous information.

Conflict of Interest: None

Financial Support: This study was supported by the National Natural Science Foundation of China (No. 82073117, Hailin Tang; 81902707, Yuehua Li) and the Science and Technology Program of Guangzhou (No. 202003000020, Hailin Tang), the Key Research Project of Hunan Provincial Education Department (21A0270, Yuehua Li), and the Natural Science Foundation of Guangdong Province (2020A1515010285, 2021A1515010547, Peng Liu).

Ethics Statement: None

References

1. Siegel RL, Miller KD, Jemal A. Cancer statistics, 2020. CA Cancer J Clin. 2020;70:7–30.
2. He Z-Y, Wu S-G, Peng F, Zhang Q, Luo Y, Chen M, et al. Up-regulation of RFC3 promotes triple negative breast Cancer metastasis and is associated with poor prognosis via EMT. Transl Oncol. 2017;10:1–9.
3. Adam R, Aloia T, Krissat J, Bralet M-P, Paule B, Giacchetti S, et al. Is liver resection justified for patients with hepatic metastases from breast cancer? Ann Surg. 2006;244:897–907 discussion 907-908.
4. Pivot X, Asmar L, Hortobagyi GN, Theriault R, Pastorini F, Buzdar A. A retrospective study of first indicators of breast cancer recurrence. Oncology. 2000;58:185–90.
5. Leung AM, Vu HN, Nguyen K-A, Thacker LR, Bear HD. Effects of surgical excision on survival of patients with stage IV breast cancer. J Surg Res. 2010;161:83–8.
6. Eng LG, Dawood S, Sopik V, Haaland B, Tan PS, Bhoo-Pathy N, et al. Ten-year survival in women with primary stage IV breast cancer. Breast Cancer Res Treat. 2016;160:145–52.
7. Liang Y, Zhang H, Song X, Yang Q. Metastatic heterogeneity of breast cancer: molecular mechanism and potential therapeutic targets. Semin Cancer Biol. 2020;60:14–27.
8. Tabariès S, McNulty A, Ouellet V, Annis MG, Dessureault M, Vinette M, et al. Afadin cooperates with Claudin-2 to promote breast cancer metastasis. Genes Dev. 2019;33:180–93.
9. Kapranov P, Cheng J, Dike S, Nix DA, Duttagupta R, Willingham AT, et al. RNA maps reveal new RNA classes and a possible function for pervasive transcription. Science. 2007;316:1484–8.
10. Chen L-L, Yang L. Regulation of circRNA biogenesis. RNA Biol. 2015;12:381–8.

11. Jeck WR, Sorrentino JA, Wang K, Slevin MK, Burd CE, Liu J, et al. Circular RNAs are abundant, conserved, and associated with ALU repeats. RNA. 2013;19:141–57.
12. Kristensen LS, Andersen MS, Stagsted LVW, Ebbesen KK, Hansen TB, Kjems J. The biogenesis, biology and characterization of circular RNAs. Nat Rev Genet. 2019;20:675–91.
13. Zhou W-Y, Cai Z-R, Liu J, Wang D-S, Ju H-Q, Xu R-H. Circular RNA: metabolism, functions and interactions with proteins. Mol Cancer. 2020;19:172.
14. Lei M, Zheng G, Ning Q, Zheng J, Dong D. Translation and functional roles of circular RNAs in human cancer. Mol Cancer. 2020;19:30.
15. Vo JN, Cieslik M, Zhang Y, Shukla S, Xiao L, Zhang Y, et al. The landscape of circular RNA in Cancer. Cell. 2019;176:869–881.e13.
16. Yu T, Wang Y, Fan Y, Fang N, Wang T, Xu T, et al. CircRNAs in cancer metabolism: a review. J Hematol Oncol. 2019;12:90.
17. Meng S, Zhou H, Feng Z, Xu Z, Tang Y, Li P, et al. CircRNA: functions and properties of a novel potential biomarker for cancer. Mol Cancer. 2017;16:94.
18. Wang Z, Yang L, Wu P, Li X, Tang Y, Ou X, et al. The circROBO1/KLF5/FUS feedback loop regulates the liver metastasis of breast cancer by inhibiting the selective autophagy of afadin. Mol Cancer. 2022;21:29.
19. Dudekula DB, Panda AC, Grammatikakis I, De S, Abdelmohsen K, Gorospe M. CircInteractome: a web tool for exploring circular RNAs and their interacting proteins and microRNAs. RNA Biol. 2016;13:34–42.
20. Enright AJ, John B, Gaul U, Tuschl T, Sander C, Marks DS. MicroRNA targets in Drosophila. Genome Biol. 2003;5:R1.
21. Vejnar CE, Zdobnov EM. MiRmap: comprehensive prediction of microRNA target repression strength. Nucleic Acids Res. 2012;40:11673–83.
22. Maragkakis M, Reczko M, Simossis VA, Alexiou P, Papadopoulos GL, Dalamagas T, et al. DIANA-microT web server: elucidating microRNA functions through target prediction. Nucleic Acids Res. 2009;37(Web Server issue):W273–6.
23. Chen Y, Wang X. miRDB: an online database for prediction of functional microRNA targets. Nucleic Acids Res. 2020;48:D127–31.
24. Agarwal V, Bell GW, Nam J-W, Bartel DP. Predicting effective microRNA target sites in mammalian mRNAs. eLife. 2015;4:e05005.
25. Jia L, Zhou Z, Liang H, Wu J, Shi P, Li F, et al. KLF5 promotes breast cancer proliferation, migration and invasion in part by upregulating the transcription of TNFAIP2. Oncogene. 2016;35:2040–51.
26. Qin J, Zhou Z, Chen W, Wang C, Zhang H, Ge G, et al. BAP1 promotes breast cancer cell proliferation and metastasis by deubiquitinating KLF5. Nat Commun. 2015;6:8471.
27. Jézéquel P, Gouraud W, Ben Azzouz F, Guérin-Charbonnel C, Juin PP, Lasla H, et al. Bc-GenExMiner 4.5: new mining module computes breast cancer differential gene expression analyses. Database (Oxford). 2021;2021:baab007.
28. Mei S, Qin Q, Wu Q, Sun H, Zheng R, Zang C, et al. Cistrome data browser: a data portal for ChIP-Seq and chromatin accessibility data in human and mouse. Nucleic Acids Res. 2017;45:D658–62.
29. Castro-Mondragon JA, Riudavets-Puig R, Rauluseviciute I, Lemma RB, Turchi L, Blanc-Mathieu R, et al. JASPAR 2022: the 9th release of the open-access database of transcription factor binding profiles. Nucleic Acids Res. 2022;50:D165–73.
30. Li J-H, Liu S, Zhou H, Qu L-H, Yang J-H. starBase v2.0: decoding miRNA-ceRNA, miRNA-ncRNA and protein-RNA interaction networks from large-scale CLIP-Seq data. Nucleic Acids Res. 2014;42(Database issue):D92–7.
31. Bray F, Ferlay J, Soerjomataram I, Siegel RL, Torre LA, Jemal A. Global cancer statistics 2018: GLOBOCAN estimates of incidence and mortality worldwide for 36 cancers in 185 countries. CA Cancer J Clin. 2018;68:394–424.
32. Ng WL, Mohd Mohidin TB, Shukla K. Functional role of circular RNAs in cancer development and progression. RNA Biol. 2018;15(8):995–1005.
33. Meng J, Chen S, Han J-X, Qian B, Wang X-R, Zhong W-L, et al. Twist1 regulates Vimentin through Cul2 circular RNA to promote EMT in hepatocellular carcinoma. Cancer Res. 2018;78:4150–62.
34. Conn SJ, Pillman KA, Toubia J, Conn VM, Salmanidis M, Phillips CA, et al. The RNA binding protein quaking regulates formation of circRNAs. Cell. 2015;160:1125–34.

35. Wang R, Zhang S, Chen X, Li N, Li J, Jia R, et al. EIF4A3-induced circular RNA MMP9 (circMMP9) acts as a sponge of miR-124 and promotes glioblastoma multiforme cell tumorigenesis. Mol Cancer. 2018;17:166.
36. Zheng X, Huang M, Xing L, Yang R, Wang X, Jiang R, et al. The circRNA circSEPT9 mediated by E2F1 and EIF4A3 facilitates the carcinogenesis and development of triple-negative breast cancer. Mol Cancer. 2020;19:73.
37. Han J, Meng J, Chen S, Wang X, Yin S, Zhang Q, et al. YY1 complex promotes quaking expression via super-enhancer binding during EMT of hepatocellular carcinoma. Cancer Res. 2019;79:1451–64.
38. Errichelli L, Dini Modigliani S, Laneve P, Colantoni A, Legnini I, Capauto D, et al. FUS affects circular RNA expression in murine embryonic stem cell-derived motor neurons. Nat Commun. 2017;8:14741.
39. Lagier-Tourenne C, Polymenidou M, Cleveland DW. TDP-43 and FUS/TLS: emerging roles in RNA processing and neurodegeneration. Hum Mol Genet. 2010;19:R46–64.
40. Han K, Wang F-W, Cao C-H, Ling H, Chen J-W, Chen R-X, et al. CircLONP2 enhances colorectal carcinoma invasion and metastasis through modulating the maturation and exosomal dissemination of microRNA-17. Mol Cancer. 2020;19:60.
41. Su J, Wang Q, Liu Y, Zhong M. miR-217 inhibits invasion of hepatocellular carcinoma cells through direct suppression of E2F3. Mol Cell Biochem. 2014;392:289–96.
42. Zhou C, Chen Y, He X, Zheng Z, Xue D. Functional implication of Exosomal miR-217 and miR-23b-3p in the progression of prostate Cancer. Onco Targets Ther. 2020;13:11595–606.
43. Li W, Yang X, Shi C, Zhou Z. Hsa_circ_002178 promotes the growth and migration of breast Cancer cells and maintains Cancer stem-like cell properties through regulating miR-1258/KDM7A Axis. Cell Transplant. 2020;29:963689720960174.
44. Liu C, Zhang Z, Qi D. Circular RNA hsa_circ_0023404 promotes proliferation, migration and invasion in non-small cell lung cancer by regulating miR-217/ZEB1 axis. OTT. 2019;12:6181–9.
45. Ben-Porath I, Thomson MW, Carey VJ, Ge R, Bell GW, Regev A, et al. An embryonic stem cell–like gene expression signature in poorly differentiated aggressive human tumors. Nat Genet. 2008;40:499–507.
46. Takagi K, Miki Y, Onodera Y, Nakamura Y, Ishida T, Watanabe M, et al. Krüppel-like factor 5 in human breast carcinoma: a potent prognostic factor induced by androgens. Endocr Relat Cancer. 2012;19:741–50.
47. Tong D, Czerwenka K, Heinze G, Ryffel M, Schuster E, Witt A, et al. Expression of *KLF5* is a prognostic factor for disease-free survival and overall survival in patients with breast Cancer. Clin Cancer Res. 2006;12:2442–8.
48. Liu R, Shi P, Zhou Z, Zhang H, Li W, Zhang H, et al. Krüpple-like factor 5 is essential for mammary gland development and tumorigenesis: KLF5 and mammary gland development. J Pathol. 2018;246:497–507.
49. Chen C, Benjamin MS, Sun X, Otto KB, Guo P, Dong X-Y, et al. KLF5 promotes cell proliferation and tumorigenesis through gene regulationin the TSU-Pr1 human bladder cancer cell line. Int J Cancer. 2006;118:1346–55.
50. Long X, Singla DK. Inactivation of Klf5 by zinc finger nuclease downregulates expression of pluripotent genes and attenuates colony formation in embryonic stem cells. Mol Cell Biochem. 2013;382:113–9.
51. Zheng H-Q, Zhou Z, Huang J, Chaudhury L, Dong J-T, Chen C. Krüppel-like factor 5 promotes breast cell proliferation partially through upregulating the transcription of fibroblast growth factor binding protein 1. Oncogene. 2009;28:3702–13.
52. Jia X, Chen H, Ren Y, Dejizhuoga, Gesangyuzhen, Gao N, et al. BAP1 antagonizes WWP1-mediated transcription factor KLF5 ubiquitination and inhibits autophagy to promote melanoma progression. Exp Cell Res. 2021;402:112506.
53. Tang J, Li Y, Sang Y, Yu B, Lv D, Zhang W, et al. LncRNA PVT1 regulates triple-negative breast cancer through KLF5/beta-catenin signaling. Oncogene. 2018;37:4723–34.
54. Gupta GP, Massagué J. Cancer metastasis: building a framework. Cell. 2006;127:679–95.
55. Heerboth S, Housman G, Leary M, Longacre M, Byler S, Lapinska K, et al. EMT and tumor metastasis. Clin Transl Med. 2015;4:6–6.

56. Brabletz T, Kalluri R, Nieto MA, Weinberg RA. EMT in cancer. Nat Rev Cancer. 2018;18:128–34.
57. Hugo H, Ackland ML, Blick T, Lawrence MG, Clements JA, Williams ED, et al. Epithelial—mesenchymal and mesenchymal—epithelial transitions in carcinoma progression. J Cell Physiol. 2007;213:374–83.
58. Zhang B, Li Y, Wu Q, Xie L, Barwick B, Fu C, et al. Acetylation of KLF5 maintains EMT and tumorigenicity to cause chemoresistant bone metastasis in prostate cancer. Nat Commun. 2021;12:1714.
59. Guo H, Ge Y, Li X, Yang Y, Meng J, Liu J, et al. Targeting the CXCR4/CXCL12 axis with the peptide antagonist E5 to inhibit breast tumor progression. Sig Transduct Target Ther. 2017;2:17033.
60. Liu D, Guo P, McCarthy C, Wang B, Tao Y, Auguste D. Peptide density targets and impedes triple negative breast cancer metastasis. Nat Commun. 2018;9:2612.
61. Yang F, Takagaki Y, Yoshitomi Y, Ikeda T, Li J, Kitada M, et al. Inhibition of Dipeptidyl Peptidase-4 Accelerates Epithelial–Mesenchymal Transition and Breast Cancer Metastasis via the CXCL12/CXCR4/mTOR Axis. Cancer Res. 2019;79:735–46.
62. Correia AL, Guimaraes JC, Auf der Maur P, De Silva D, Trefny MP, Okamoto R, et al. Hepatic stellate cells suppress NK cell-sustained breast cancer dormancy. Nature. 2021;594:566–71.